Intrinsic Zero-Linear and Zero-Area Compressibility over an Ultra-Wide Pressure Range within a "*Gear-Spring*" Structure

Dequan Jiang
Center for High Pressure Science and Technology Advanced Research https://orcid.org/0000-0003-0998-5507

Ting Wen
Center for High Pressure Science and Technology Advanced Research

Huimin Song
Center of Materials Science and Optoelectronics Engineering, University of Chinese Academy of Sciences

Zimin Jiang
Center for High Pressure Science and Technology Advanced Research (HPSTAR)

Chen Li
Center for High Pressure Science and Technology Advanced Research (HPSTAR)

Ke Liu
Center for High Pressure Science and Technology Advanced Research (HPSTAR)

Wenge Yang
Center for High Pressure Science and Technology Advanced Research https://orcid.org/0000-0001-8436-8731

Ho-Kwang Mao
Center for High Pressure Science and Technology Advanced Research

Yonggang Wang (yonggang.wang@hpstar.ac.cn)
Center for High Pressure Science and Technology Advanced Research (HPSTAR)
https://orcid.org/0000-0003-4816-9182

Article

Keywords: Rotatable Metal Coordination Polyhedra, Mechanical Unloading Device, Anisotropic Compression Materials, Shock-resistant Precision Optics

Posted Date: July 2nd, 2021

DOI: https://doi.org/10.21203/rs.3.rs-588081/v1

Version of Record: A version of this preprint was published at CCS Chemistry on January 17th, 2022. See the published version at https://doi.org/10.31635/ccschem.022.202101739.

Abstract

Materials with zero-linear compression (ZLC) and zero-area compression (ZAC) hold great promises for specific applications retaining constant in specific directions or planes under external impaction. Up to now, no more than ten ZLC/ZAC materials have been reported, most of which are of very limited working pressure ranges (< 10 GPa). Herein, we report the observation of concurrent ZLC and ZAC in $Li_2Ti(IO_3)_6$ with a "*Gear-Spring*" type structure over an ultra-wide pressure range (0 ~ 40 GPa). Structure analysis reveals that the rotatable metal coordination polyhedra (gears) and extremely compressible metal chains (springs) work together to form an exquisite mechanical unloading device with intrinsic ZLC and ZAC behavior. Moreover, $Li_2Ti(IO_3)_6$ sets a record-wide ZLC/ZAC working pressure range (up to 40 GPa) among anisotropic compression materials. The demonstration of intrinsic and long-lasting ZLC/ZAC with a "*Gear-Spring*" mechanism paves the way to shock-resistant precision optics applied under extreme conditions.

Introduction

Substances normally contract under external hydrostatic pressure, just as they expand with heat and contract with cold.[1,2] From the perspective of thermodynamics, it is impossible for a given material exhibiting negative volume compressibility.[3] Nevertheless, there are several types of materials possessing negative compressibility in specific crystalline directions or planes, while the overall cell volume keeps decreasing under compression.[4-6] In the past decades, materials with negative linear compressibility (NLC) and negative area compressibility (NAC) have been widely explored with specific mechanisms, such as "*wine-rack*", honeycomb networks, and *Lifshitz* model.[7-9] In general, zero linear compressibility (ZLC) and zero area compressibility (ZAC) can be easily achieved by finding a balance between negative and positive compressibility, and the linear and area compressibility of diamond and Os are used as standard to classify a ZLC or ZAC material.[10-13] ZLC and ZAC materials are ideal candidates for precision instruments applied under extreme environments, such as submarine fiber-optic communication and shock-resistant optical windows.[1,14,15] Surprisingly, material with ZLC or ZAC has been rarely discovered compared with those of NLC and NAC property.[9,10,16-19] Meanwhile, there lacks clear structure-property mechanism for the rational design of ZLC/ZAC materials.

In the decade's exploration of materials with abnormal compressibility, remarkable findings have been concentrated in two types of materials: metal-organic frameworks (MOFs) and all-inorganic frameworks.[4] The most important strategy to achieve materials with abnormal compressibility is to establish clear and instructive structure-property relationship. The diverse organic units endow MOFs the ability to exhibit flexible mechanical responses under compression,[20-23] including both large NLC and near-ZLC. The "*wine racks*" structure model is the most popular mechanism describing the NLC and near-ZLC behaviors in MOFs. Particularly, "molecular gears and torsion springs" structure model is proposed to describe the NLC and extreme compressibility of $LnFe(CN)_6$ (*Ln* = Ho, Lu or Y), which benefit from the LnN_6 torsion springs and the rigid $Fe(CN)_6$ gears.[24] However, MOFs are soft and usually show above-mentioned abnormal

compressibility within a very narrow pressure range, typically no more than 10 GPa, which greatly limits their potential applications. Comparatively, all-inorganic frameworks such borates possessing covalently-bonded frameworks are less compressible. Although up to now the highest pressure of ZLC is 8 GPa in $(Ca,Sr)B_2O_4$, from the viewpoint of structural chemistry, they are still good candidates with abnormal compressibility in a relatively wide pressure range.[4] In addition, all-inorganic frameworks can have good chemical/physical stability and excellent optical performances, which makes them potential for next-generation shock-resistant optical windows and fiber communications. Unfortunately, there lacks clear mechanism for the rational design of all-inorganic frameworks with abnormal compressibility. An exception is the recently reported "*Lu-Ban Stool*"-like model for $(Ca,Sr)B_2O_4$, in which the subtle counterbalance originated from the expansion and contraction effect between the rotation of the $[BO_3]$ "planks" and the shrinkage of Ca-O "legs" attributes to an excellent ZLC property.[10]

We are aiming at exploring all-inorganic optical materials with both excellent ZLC/ZAC properties and good chemical/physical stabilities by structure design strategy. Numerous known inorganic compounds in the ICSD database have been screened to look for framework-like structures, among which a unique family of transition metal iodates with metal-metal bonding and chains are identified potential for ZLC/ZAC behavior. Herein, we report the anomalous mechanical responses of $Li_2Ti(IO_3)_6$ to external pressure as a representative of inorganic framework structure. The anisotropic compressibility of $Li_2Ti(IO_3)_6$ was examined by using *in-situ* X-ray diffraction (XRD), Raman spectra, and first-principles calculations. A "*Gear-Spring*" mechanism was proposed responsible for the emerging intrinsic ZLC/ZAC properties, which sheds light on the future structure design of all-inorganic materials with anomalous compressibility.

Results And Discussion

Material and Ambient Crystal Structure. Phase-pure $Li_2Ti(IO_3)_6$ were obtained by hydrothermal method as both white powders and transparent single crystals. At ambient conditions, $Li_2Ti(IO_3)_6$ crystallizes in the hexagonal space group $P6_3$ with cell parameters of a = 9.372 Å, c = 5.113 Å (Fig. S1). Fig. 1a shows the crystal structure of $Li_2Ti(IO_3)_6$ consisting of face-sharing TiO_6 chains along the c-axis, distorted IO_3 units and LiO_6 octahedra. The structure is noncentrosymmetric with a very strong second harmonic generation (SHG) efficiency of ~500 × α-SiO_2, comparable to those of $BaTiO_3$ (400 × α-SiO_2) and $LiNbO_3$ (600 × α-SiO_2).[25] Both the Ti^{4+} and I^{5+} cations are located within asymmetric coordination environments due to the second-order Jahn-Teller effects. The parallel alignment of the lone pair electrons on the I^{5+} cations contributes mostly to the macroscopic polarity of $Li_2Ti(IO_3)_6$ (Fig. S2).[26,27] Notably, each TiO_6 octahedron links with six IO_3 polyhedra to form a large anionic $[(TiO_{6/2})^{2-}{\cdot}6(IO_{1/2}O_{2/1})^0]^{2-}$ "cylinder" in the *ab* plane, and these nano-cylinders are seperated by six-coordinated Li^+ cations to acheive charge balance. In such an inorganic framework, the "cylinders" are experected to have the ability to "rotate" around the Ti-Ti axis since the connection manner between $(TiO_{6/2})^{2-}$ and six $(IO_{1/2}O_{2/1})^0$ is corner-sharing. Thus, one can

consider the anionic $[(TiO_{6/2})^{2-}\cdot 6(IO_{1/2}O_{2/1})^{0}]^{2-}$ to be a rigid "roller". Previous studies have preliminarily verified the anomalous compressiblity of similar metal iodates such as $Fe(IO_3)_3$ and $Zn(IO_3)_2$.[28,29] We have enough reasons to expect peculiar mechanical responses of $Li_2Ti(IO_3)_6$ to external pressure.

Structure Evolution of $Li_2Ti(IO_3)_6$ under High Pressure. *In-situ* high-pressure XRD measurements were conducted to study the compressibility of $Li_2Ti(IO_3)_6$ with the "inorganic-framework" structure (Fig. 1b). No obvious structural phase transition is observed under compression up to 40.2 GPa since there is only peak shift instead of new peak emerging or disappear, and the pressure effect on the crystal structure is reversible (Fig. S3). Different Bragg peaks exhibit obviously distinct shift behaviors under compression, implying an extremely anisotropic compressibility along different crystallographic axes. Among them, the (*hk*0) peaks such as (2 0) and (300) basically keep their 2θ values unchanged, indicating an incompressibility or minimal compressibility along the *a* and *b* axes. Specifically, the (*hk*0) peaks shift slightly to lower 2θ angle first in the 0~8 GPa range (*i*), and then slightly to higher 2θ angle in the 8~19 GPa (*ii*), and finally to lower 2θ angle again above 19 GPa (*iii*) (Fig. S4). By contrast, the (*hkl*) peaks such as (2 1) with $l \neq 0$ shift quickly to higher 2θ angle under compression up to 40 GPa, indicating a large compressibility along the *c* axis.

Fig. 1c and Table S1 displays the refined cell parameters of $Li_2Ti(IO_3)_6$ as functions of applied pressure. The extremely anisotropic compression behavior is evident. The evolution of the *a* axis has gone through three pressure regions in accordance with the peak shift of the (*hk*0) planes. Notably, the overall change of the *a* axis (Δa) in the 0~40.2 GPa region is as low as 0.97%, a low enough value to be regarded as ZLC. Due to the hexagonal symmetry of space group $P6_3$ with $a = b$, the *ab* plane exhibits similar compression behavior with individual *a* and *b* axes, *i.e.* the overall area change of the *ab* plane (Δs) in the 0~40.2 GPa is as low as 1.95%, which is also a low enough value to be ZAC. Comparatively, *c* axis exhibits tremendous compressibility with $\Delta c = 28.69\%$ at 40.2 GPa, and a normal *V-P* curve is obtained in the whole pressure range.

Table 1. The compressibility and pressure range in all reported ZAC/ZLC materials.

Material	Mechanism	K_l (TPa^{-1})	K_s (TPa^{-1})	P (GPa)	*Ref.*
MIL-122(In)	"*Wine-rack*"	0	/	0~10.5	[18]
$[C(NH_2)_3][Cd(HCOO)_3]$	"*Wine-rack*"	0.75	1.51	0~0.5	[17]
SrB_2O_4	"*Lu-Ban Stool*"	-0.47	/	0~8.0	[10]
CaB_2O_4	"*Lu-Ban Stool*"	0.34	/	0~8.1	[10]
$LiBO_2$	"*Corrugated-graphite*"	1.54	/	0~2.5	[16]
$RbBe_2BO_3F_2$	"*Lifshitz*"	0.05	0.1	0~2.6	[9]
$CsBe_2BO_3F_2$	"*Lifshitz*"	-0.03	-0.07	0~3.2	[9]
GeO_2	/	0.08	/	0~8.0	[19]
Dimond	*Superhard*	0.62	1.23	0~45.0	[11]
Os	*Superhard*	0.60[a] 0.54[c]	1.02	0~63.8	[13]
$Li_2Ti(IO_3)_6$	**"*Gear-Spring*"**	**0.24**	**0.48**	**0~40.2**	**This work**

ZLC and ZAC of $Li_2Ti(IO_3)_6$. The linear compressibility (K_l) has been defined as $-dl/ldp$ to evaluate the strength of mechanical response to external pressure of a given material.[4] Fig. 1d represents the pressure-dependent linear compressibilities ($K_{a/b}$ and K_c) of $Li_2Ti(IO_3)_6$, derived using the online PASCal package[30] and within three above-discussed pressure ranges (*i*, *ii*, *iii*). It is interesting to see that $K_{a/b}$ keeps very small values throughout the whole pressure range. The calculated values for individual pressure ranges are: K_a = 1.06 TPa^{-1} and K_c = 10.54 TPa^{-1} for *i*, (0~8 GPa); K_a = -1.88 TPa^{-1} and K_c = 14.84 TPa^{-1} for *ii*, (8~19 GPa); K_a = 0.58 TPa^{-1} and K_c = 1.78 TPa^{-1} for *iii* (19~40.2 GPa), respectively (Fig. S5). Notably, the positive K_a in the *i* (0~8 GPa) range and the negative K_a in the *ii* (8~19 GPa) range yield a very small K_a value of -0.23 TPa^{-1} in the *i*+*ii* region (0~19 GPa). According to the previous definition, compounds with absolute value of K_l less than those of diamond (0.75 TPa^{-1}) and Os (0.70 TPa^{-1}) can be considered as ZLC materials. Thus, $Li_2Ti(IO_3)_6$ is a novel ZLC material in both *a* and *b* directions in the pressure range of 0~40.2 GPa. Of cause, $Li_2Ti(IO_3)_6$ is also a novel ZAC material since the area change of the *ab* plane (Δs) is as low as 1.95% within 0~40.2 GPa.

The online PASCal package is found only applicable to those cases with either a positive or a negative K_l. To calculate the total K_l for our case with both positive and negative linear compressibilities in a pressure range, we simply use the most primitive formulas ($K_l = -\Delta l/l\Delta p$ and $K_s = -\Delta s/s\Delta p$) to evaluate the linear and area compressibilities, where *l* represents the length of the starting unit cell, *s* represents the area of

the initial crystal plane, Δ*l*, Δ*s* and Δ*p* represents the changes of linear, area and pressure, respectively. The recalculated K_a and K_s in the pressure range of 0~40.2 GPa are provided in Fig. S6, and the compressive properties of representative ZLC/ZAC materials including the superhard diamond and Os as references are concluded in Table 1.

First of all, $Li_2Ti(IO_3)_6$ possesses relatively small K_l (0.24 TPa^{-1}) and K_s (0.48 TPa^{-1}) within these materials including diamond (K_l = 0.62 TPa^{-1}, K_s = 1.23 TPa^{-1}) and Os metal (K_l = 0.54/0.60 TPa^{-1}, K_s = 1.02 TPa^{-1}), making it worthy of ZLC and ZAC material. Remarkably, inorganic ceramics or crystalline materials with both ZAC property and transparency in important wavelengths are rather rarely reported up to now, which holds great promise for practical shock-resistant optical usages. Secondly, $Li_2Ti(IO_3)_6$ exhibits ZLC and ZAC in an ulta-wide pressure range, *i.e.* 0~40.2 GPa, compared with ZLC/ZAC MOFs and metal borates. 40.2 GPa may not be the highest pressure value for $Li_2Ti(IO_3)_6$ to survive, nevertheless, this value still refreshes the world record of ZLC/ZAC material (except diamond and Os). At last, as we know, there are several structural mechanisms for previously discovered ZLC/ZAC materials, such as "*Wine-rack*" for MOFs, "*Lu-Ban Stool*"/"*Corragated graphite*"/"*Lifshitz*" for some borates, and *superhard* for diamond and Os, respectively. However, $Li_2Ti(IO_3)_6$ does not belong to any of the above-mentioned mechanisms.

Intrinsic ZLC/ZAC in "*Gear-Spring*" structures. The crystal structure of $Li_2Ti(IO_3)_6$ can be vividly regarded as a "*Gear-Spring*" type. As shown in Fig. 2a, the visualized "*Gear-Spring*" model of $Li_2Ti(IO_3)_6$ comprises of Gear-A (the anionic $[(TiO_{6/2})^{2-}\cdot 6(IO_{1/2}O_{2/1})^{0}]^{2-}$), Gear-B ($LiO_6$ octahedra), and an extremely compressible spring (Ti-Ti distances or *c*). This model is completely derived from the real crystal structure and can describe and explain the ZLC/ZAC phenonmena of $Li_2Ti(IO_3)_6$ perfectly.

The parameters of the "*Gear-Spring*" model, gear radii (r(Gear-A), r(Gear-B)), spring length (*c*) and rotation angles (θ(Gear-A), θ(Gear-B)) were derived from structure optimization using the experimental cell parameters of $Li_2Ti(IO_3)_6$ under various pressures. As rigid "gears", the sizes of "Gear-A" and "Gear-B" should basically remain unchanged, which has been perfectly validated by the calculation results (Fig. 2b). In the meantime, the spring length (*c*) decearses rapidly along with the increasing of applied pressure, working together as real springs. It is really amazing that the two gears (A and B) can rotate synergistically either in the direction or angles (Fig. 2c). A little different from the previously derived three pressure regions (*i*, *ii*, *iii*) of the cell parameter evolusion, four rotation processes are observed under compression: (*i*) A^+(counterclockwise)B^-(clockwise) in 0~9 GPa, (*ii*-a) A^+B^+ in 9~14 GPa, (*ii*-b) A^-B^+ in 14~17 GPa, and (*iii*) A^0B^0 in 17~40 GPa, respectively. It is reasonable to believe that the rotation of the gears can convert the external pressure to the compression direction of the spring.

Fig. 2d displays the representive structures of the TiO_6-chain at 0 GPa and the highest pressure 40.2 GPa. The working mechanism of the "spring" is clear from the dramatic changes of the Ti-Ti ditances and Ti-O-Ti bond angles. The *c* value (spring length) is reduced from 5.07 Å to 3.63 Å, together with highly flattened Ti-O-Ti angle (from 81.3° to 52.4°) but almost unchanged Ti-O bondlengths (from 1.92/2.01 Å

to 2.04/2.07 Å). The detailed changes of individual bondlengths during the "*Gear-Spring*" working process under compression are displayed in Fig. 2e, 2f. Both the Ti-Ti distances and Ti-O-Ti angles exhibit similar changes under compression up to 40 GPa, and there is no distortion from the Ti-O bondlengths within TiO_6 octahedra. The average bondlengths of I-O and Ti-O also show cooperative changes under high pressure to maintain the size of Gear-A unchanged. In brief, the emerging ZLC/ZAC phenomena in $Li_2Ti(IO_3)_6$ can be perfectly explained by the "*Gear-Spring*" mechanism. Materials with such a "gear" and "spring" cooperation structure are expected to have intrinsic ZLC/ZAC properties, and also in an ultra-wide pressure range.

The local structure evolution of $Li_2Ti(IO_3)_6$ during ZLC/ZAC processes are probed by *in-situ* high-pressure Raman spectra (Fig. S7). Firstly, the Raman profile bacially remains unchange under compression except gradual shifts of the peaks, indicating the absence of structural phase transition. The peaks located in the ranges of 400-600 and 600-850 cm^{-1} can be assigned to the stretching vibration modes of $[TiO_6]$ octahedra and $[IO_3]$ pyramids, respectively. The softening of the $[IO_3]$ peaks (shift continuouly to lower wavenumber) indicates the elongation of the I-O bonds. Besides, we also measured the SHG efficiency of $Li_2Ti(IO_3)_6$ powders under high pressure (Fig. S8). It is interesting to find that $Li_2Ti(IO_3)_6$ keeps to be SHG-active up to 40.2 GPa. The long-lasting SHG functionality combined with intrinsic ZLC/ZAC properties within an ulta-wide pressure range makes $Li_2Ti(IO_3)_6$ a unique candidate for optically sensitive devices under extreme conditions.

Conclusion

In summary, we report intrinsic ZLC and ZAC properties in an all-inorganic iodate material $Li_2Ti(IO_3)_6$. The ultra-wide working pressure range (0~40.2 GPa) of $Li_2Ti(IO_3)_6$ sets a new record for artificial ZLC or ZAC materials (except diamond and Os). Based on structure analyses, we proposed a novel "*Gear-Spring*" mechanism that can describe and explain the anomolous compression behavior of $Li_2Ti(IO_3)_6$ perfectly. We are confident to predict anomolous compression properties (including intrinsic ZLC and ZAC) in compounds with such a "*Gear-Spring*" structure. Moreover, $Li_2Ti(IO_3)_6$ maintains its nonlinear optical functionality along with ZLC/ZAC behavior to high pressure, which makes it promising for special optical devices under extreme environments.

Methods

Sample preparation. Reagents: Li_2CO_3 (Aladdin, 99.99%), TiO_2 (Aladdin, 99.99%), HIO_3 (Aladdin, 99.99%). Powders and single crystals of $Li_2Ti(IO_3)_6$ were synthesized by hydrothermal method. Li_2CO_3 (0.30 g, 4.06×10^{-3} mol), TiO_2 (0.300 g, 3.76×10^{-3} mol), HIO_3 (5.00 g, 2.84×10^{-2} mol) and water (10 mL) were put in a 23 mL Teflon-lined stainless steel autoclave and heated to 230 °C for 4 days followed by cooling to room temperature with the rate of 3 °C/h. Transparent, colorless crystals and white powder of $Li_2Ti(IO_3)_6$ were washed by water and ethanol, and dried at 70 ^oC overnight.

High-pressure generation. A symmetric diamond-anvil-cell (DAC) was used to produce high pressure. T301 steel gaskets were pressed to the thickness of about 35 μm, and then 180 μm holes were drilled as the sample chambers. Compact sample and a ruby ball were thrown into the sample chamber. Silicone oil was employed as the pressure medium. The pressure was calibrated based on the fluorescence peak of ruby ball.[31]

High-pressure XRD measurement. *In-situ* high-pressure XRD experiments were recorded at the 4W2 High Pressure Station in Beijing Synchrotron Radiation Facility (BSRF) with a beam wavelength of 0.6199 Å at room temperature. A Mar345 image plate was used to record the *in-situ* high-pressure XRD patterns, and CeO_2 was chosen as the calibration standard. DIOPTAS software was used to execute the data reduction.[32] Cell parameters under different pressures were refined by Rietveld method using the FULLPROF software.[33] The compressibility was calculated by the empirical function $I = I_0 + \lambda (p - p_c)^{\upsilon}$ via the online program PASCal (http://pascal.chem.ox.ac.uk/).[30]

High-pressure Raman measurement. *In-situ* high-pressure Raman spectra were recorded on a Renishaw Raman microscope using a 532 nm laser. The system was calibrated by the Raman signal of Si, and spectra were collected in the range of 100-1100 cm^{-1}.

High-pressure SHG measurement. *In-situ* high-pressure SHG experiment was measured in a home-designed optical system. A fiber laser (NPI LASERCo., Ltd, 1064 nm, 20MHz, 15 ps) was used as the exciting light source, and the laser spot was focused to 40 μm. A photomultiplier tube (Thorlabs, Inc., PMT1000) was employed to collect the SHG signal. The high-pressure SHG measurement is based on the ambient powder SHG measurement extended by Kurtz and Perry.[34]

First-principles calculation. The first-principles calculation was performed using the CASTEP package.[35] Structure optimization at various pressure points was performed adopting the experimental cell sizes with all the atomic positions relaxed.

Data availability

The data that support the findings of this study are available in the Supplementary Information (experimental data and characterization data). All raw data and analysis files used in the study are available upon request from the authors.

Declarations

Acknowledgement

This work was supported by National Natural Science Foundation of China (52073003), Major Program of National Natural Science Foundation of China (22090041), National Key R&D Program of China (2018YFA0305900). High-pressure XRD data were collected at beamline station 4W2 of Beijing Synchrotron Radiation Facility (SSRF), Beijing, China.

Author contributions

D.J., T.W. and Y.W. conceived the idea and led the project. D.J. and H.S. conducted the synthesis, crystal growth and structure refinement. Z. J. and W.T. performed high-pressure XRD measurement. C.L. and K. L. performed high-pressure Raman and SHG measurements. D.J., T.W. and Y.W. wrote the manuscript with help from W.Y. and H.M. All authors discussed and revised the manuscript.

Competing interests

The authors declare no competing interests.

Correspondence and requests for materials should be addressed to T.W. and Y. W.

References

1. Grima, J. N. & Caruana-Gauci, R. Materials that push back. *Nat. Mater.* **11**, 565-566 (2012).

2. Lakes, R. Foam Structures with a Negative Poisson's Ratio. *Science* **235**, 1038-1040 (1987).

3. Baughman, R. H., Stafström, S., Cui, C. & Dantas, S. O. Materials with Negative Compressibilities in One or More Dimensions. *Science* **279**, 1522-1524 (1998).

4. Cairns, A. B. & Goodwin, A. L. Negative linear compressibility. *Phys. Chem. Chem. Phys.* **17**, 20449-20465 (2015).

5. Fortes, A. D., Suard, E. & Knight, K. S. Negative Linear Compressibility and Massive Anisotropic Thermal Expansion in Methanol Monohydrate. *Science* **331**, 742-746 (2011).

6. Zeng, Q., Wang, K. & Zou, B. Large Negative Linear Compressibility in $InH(BDC)_2$ from Framework Hinging. *J. Am. Chem. Soc.* **139**, 15648-15651 (2017).

7. Cairns, A. B., Catafesta, J., Levelut, C., Rouquette, J., Lee, A., Peters, L., Thompson, A. L., Dmitriev, V., Haines, J. & Goodwin, A. L. Giant negative linear compressibility in zinc dicyanoaurate. *Nat. Mater.* **12**, 212-216 (2013).

8. Goodwin, A. L., Keen, D. A. & Tucker, M. G. Large negative linear compressibility of $Ag_3[Co(CN)_6]$. *Proc. Natl. Acad. Sci. U. S. A.* **105**, 18708-18713 (2008).

9. Jiang, X., Luo, S., Kang, L., Gong, P., Yao, W., Huang, H., Li, W., Huang, R., Wang, W., Li, Y., Li, X., Wu, X., Lu, P., Li, L., Chen, C. & Lin, Z. Isotropic Negative Area Compressibility over Large Pressure Range in Potassium Beryllium Fluoroborate and its Potential Applications in Deep Ultraviolet Region. *Adv. Mater.* **27**, 4851-4857 (2015).

10. Jiang, X., Yang, Y., Molokeev, M. S., Gong, P., Liang, F., Wang, S., Liu, L., Wu, X., Li, X., Li, Y., Wu, S., Li, W., Wu, Y. & Lin, Z. Zero Linear Compressibility in Nondense Borates with a “Lu-Ban Stool”-Like Structure. *Adv. Mater.* **30**, 1801313 (2018).

11. Occelli, F., Loubeyre, P. & LeToullec, R. Properties of diamond under hydrostatic pressures up to 140 GPa. *Nat. Mater.* **2**, 151-154 (2003).

12. Cynn, H., Klepeis, J. E., Yoo, C. S. & Young, D. A. Osmium has the lowest experimentally determined compressibility. *Phys. Rev. Lett.* **88**, 135701 (2002).

13. Godwal, B. K. Yan, J. Clark, S. M. & Jeanloz, R. High-pressure behavior of osmium: An analog for iron in Earth’s core. *J. Appl. Phys.* **111**, 112608 (2012).

14. Evans, K. E. & Alderson, A. Auxetic Materials: Functional Materials and Structures from Lateral Thinking! *Adv. Mater.* **12**, 617-628 (2000).

15. Baughman, R. H. Auxetic materials: Avoiding the shrink. *Nature* **425**, 667 (2003).

16. Jiang, X., Molokeev, M. S., Dong, L., Dong, Z., Wang, N., Kang, L., Li, X., Li, Y., Tian, C., Peng, S., Li, W. & Lin, Z. Anomalous mechanical materials squeezing three-dimensional volume compressibility into one dimension. *Nat. Commun.* **11**, 5593 (2020).

17. Zeng, Q., Wang, K. & Zou, B. Near Zero Area Compressibility in a Perovskite-Like Metal-Organic Frameworks $[C(NH_2)_3][Cd(HCOO)_3]$. *ACS Appl. Mater. Interfaces* **10**, 23481-23484 (2018).

18. Yu, Y., Zeng, Q., Chen, Y., Jiang, L., Wang, K. & Zou, B. Extraordinarily Persistent Zero Linear Compressibility in Metal-Organic Framework MIL-122(In). *ACS Materials Lett.* **2**, 519-523 (2020).

19. Haines, J., Léger, J. M., Chateau, C. & Pereira, A. S. Structural evolution of rutile-type and $CaCl_2$-type germanium dioxide at high pressure. *Phys. Chem. Minerals* **27**, 575-582 (2000).

20. Horike, S., Shimomura, S. & Kitagawa, S. Soft porous crystals. *Nat. Chem.* **1**, 695 (2009).

21. Ortiz, A. U., Boutin, A., Fuchs, A. H. & Coudert, F. X. Anisotropic elastic properties of flexible metal-organic frameworks: how soft are soft porous crystals? *Phys. Rev. Lett.* **109**, 195502 (2012).

22. Mellot-Draznieks, C., Serre, C., Surble, S., Audebrand, N. & Ferey, G. Very large swelling in hybrid frameworks: a combined computational and powder diffraction study. *J. Am. Chem. Soc.* **127**, 16273-16278 (2005).

23. Maji, T. K., Matsuda, R. & Kitagawa, S. A flexible interpenetrating coordination framework with a bimodal porous functionality. *Nat. Mater.*, **6**, 142-148 (2007).

24. Duyker, S. G., Peterson, V. K., Kearley, G. J., Studer, A. J. & Kepert C. J. Extreme compressibility in $LnFe(CN)_6$ coordination framework materials via molecular gears and torsion springs. *Nat. Chem.* **8**, 270-275 (2016).

25. Chang, H.-Y., Kim, S.-H., Halasyamani, P. S. & Ok, K. M. Alignment of Lone Pairs in a New Polar Material: Synthesis, Characterization, and Functional Properties of $Li_2Ti(IO_3)_6$. *J. Am. Chem. Soc.* **131**, 2426-2427 (2009).

26. Hu, C.-L. & Mao, J.-G. Recent advances on second-order NLO materials based on metal iodates. *Coord. Chem. Rev.* **288**, 1-17 (2015).

27. Chen, J., Hu, C.-L., Mao, F.-F., Yang, B.-P., Zhang, X.-H. & Mao, J.-G. REI_5O_{14} (RE=Y and Gd): Promising SHG Materials Featuring the Semicircle-Shaped $I_5O_{14}^{3-}$ Polyiodate Anion. *Angew. Chem. Int. Ed.* **58**, 11666-11669 (2019).

28. Liang, A., Rahman, S., Saqib, H., Rodriguez-Hernandez, P., Muñoz, A., Nénert, G., Yousef, I., Popescu, C. & Errandonea, D. First-Order Isostructural Phase Transition Induced by High Pressure in $Fe(IO_3)_3$. *J. Phys. Chem. C* **124**, 8669-8679 (2020).

29. Liang, A., Popescu, C., Manjon, F. J., Rodriguez-Hernandez, P., Muñoz, A., Hebboul, Z. & Errandonea, D. Structural and vibrational study of $Zn(IO_3)_2$ combining high-pressure experiments and density-functional theory. *Phys. Rev. B* **103**, 054102 (2021).

30. Cliffe, M. J. & Goodwin, A. L. *PASCal*: a principal axis strain calculator for thermal expansion and compressibility determination. *J. Appl. Cryst.* **45**, 1321-1329 (2012).

31. Mao, H. K., Xu, J. & Bell, P. M. Calibration of the ruby pressure gauge to 800 kbar under quasihydrostatic conditions. *J. Geophys. Res.* **91**, 4673-4676 (1986).

32. Prescher, C. & Prakapenka, V. B. DIOPTAS: A Program for Reduction of Two-Dimensional X-Ray Diffraction Data and Data Exploration. *High Pressure Res.* **35**, 223-230 (2015).

33. Rodriguez-Carvajal, J. Recent advances in magnetic structure determination by neutron powder diffraction. *Physica B* **192**, 55-69 (1993).

34. Kurtz, S. K. & Perry, T. T. A Powder Technique for the Evaluation of Nonlinear Optical Materials. *J. Appl. Phys.* **39**, 3798-3813 (1968).

35. Clark, S. J., Segall, M. D., Pickard, C. J., Hasnip, P. J., Probert, M. J., Refson, K. & Payne, M. C. First principles methods using CASTEP. *Z. Kristallogr.* **220**, 567-570 (2005).

Figures

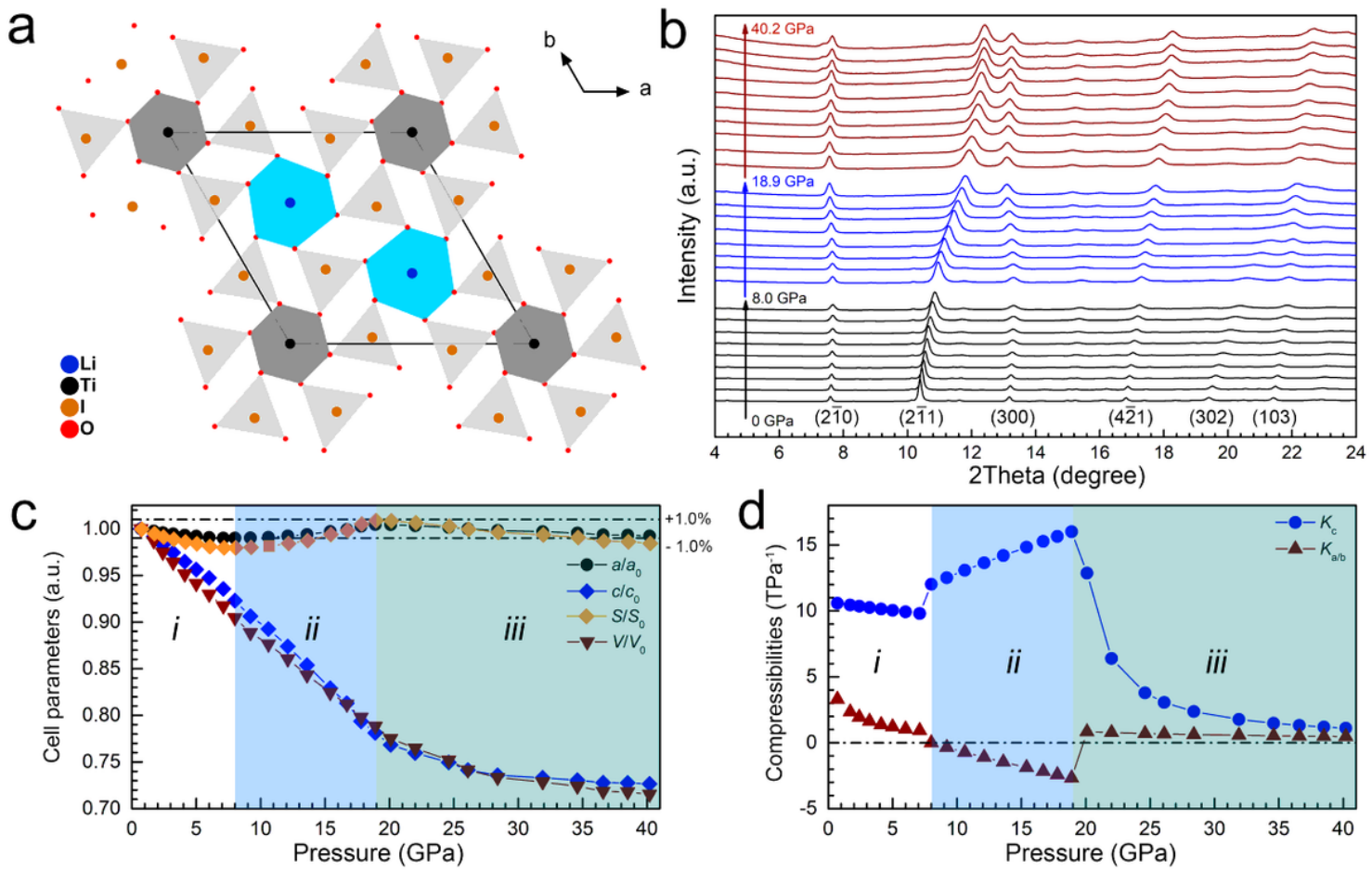

Figure 1

Crystal structure and compression behavior of Li2Ti(IO3)6. (a) Hexagonal structure of Li2Ti(IO3)6 at ambient conditions, consisting of face-sharing TiO6 chain (dark gray) along the c-axis, distorted IO3 units (light gray) and LiO6 octahedra (blue). (b) XRD patterns of Li2Ti(IO3)6 at high pressures. The anisotropic compressibility is evident without structural phase transition. (c) Cell parameters and volume as functions of pressure, showing intrisinc ZLC and ZAC behavior along the a/b directions and in the ab plane, respectively. The dotted lines represent the change of cell parameters and volume within a very small range (±1%). (d) Pressure-dependent linear compressibilities (Ka/b and Kc) of Li2Ti(IO3)6, calculated using the online PASCal package.30

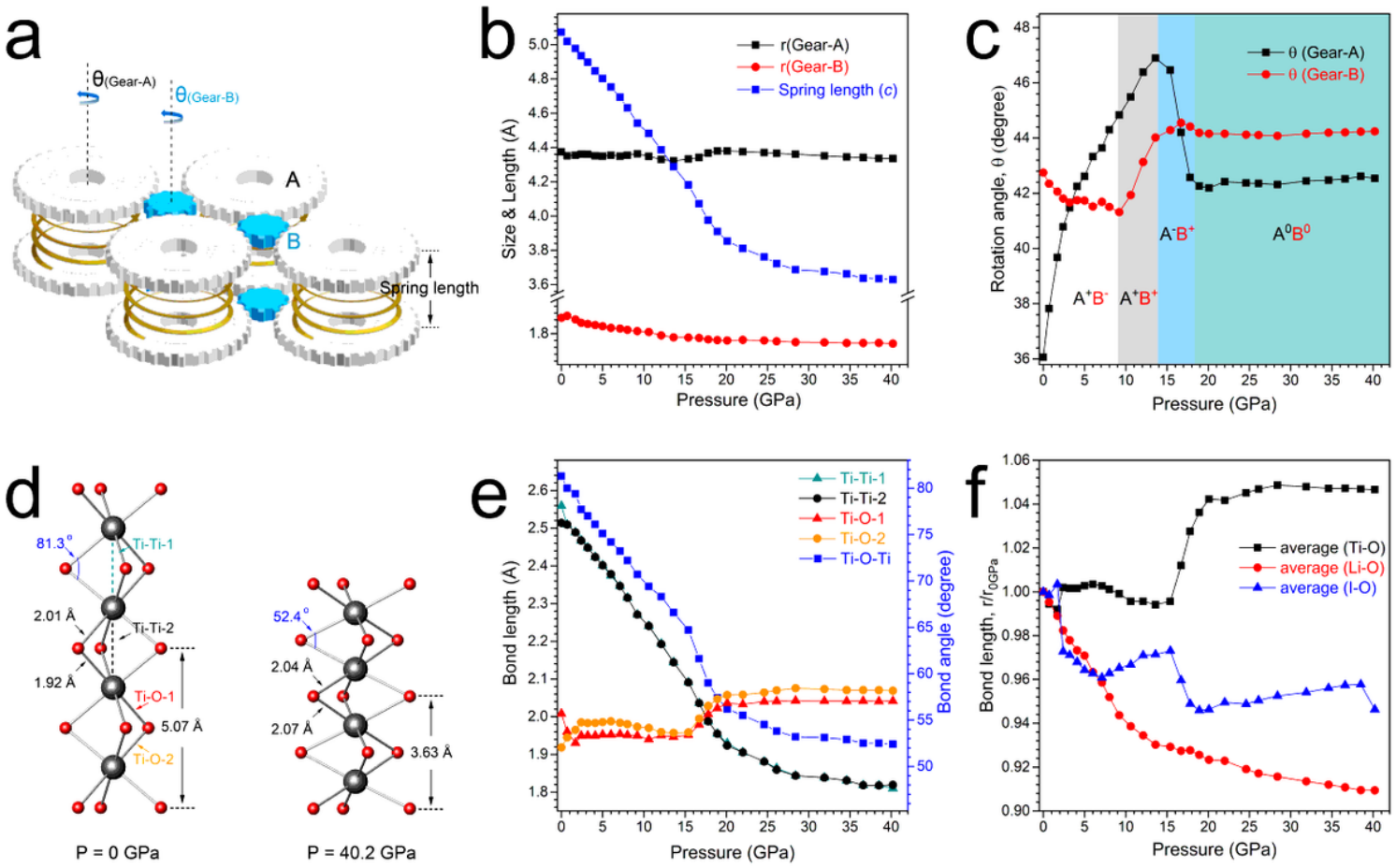

Figure 2

"Gear-spring" mechanism for ZLC/ZAC under compression. (a) Visualized "Gear-spring" structure of Li2Ti(IO3)6, comprising of Gear-A (the anionic [(TiO6/2)2-·6(IO1/2O2/1)0]2-), Gear-B (LiO6 octahedra), and the extremely compressible spring-length (Ti-Ti distances or c). (b) Evolusions of the size and length of Gear-A, Gear-B, and spring under compression. The "gears" are expected to keep their sizes and the "springs" are expected to exhibit extreme large compressibility. (c) Pressure-dependent rotations of Gear-A and Gear-B. "+" indicates anticlockwise and "-" indicates clockwise. (d) Representive structures of the TiO6-chain at 0 GPa and 40.2 GPa, showing the working mechanism of the "spring". (e, f) Bond-length and bond-angle evolusions in the "Gear-Spring" structure of Li2Ti(IO3)6 under compression.

Supplementary Files

This is a list of supplementary files associated with this preprint. Click to download.

- Graphicalabstract.docx
- LTIOSI.docx